Journal of Southeast University (English Edition) Vol. 23, No. 2, pp. 151 – 155 June 2007 ISSN 1003—7985

On-body propagation characterization based on FDTD method for 2.4/5.2/5.7 GHz wearable body sensor networks

Bao Shudi[1,2] Shen Lianfeng[1] Zhang Yuanting[2]

([1]National Mobile Communications Research Laboratory, Southeast University, Nanjing 210096, China)

([2]Joint Research Centre for Biomedical Engineering, The Chinese University of Hong Kong, Hong Kong, China)

Abstract: The on-body path loss and time delay of radio propagation in 2.4/5.2/5.7 GHz wearable body sensor networks (W-BSN) are studied using Remcom XFDTD, a simulation tool based on the finite-difference time-domain method. The simulation is performed in the environment of free space with a simplified three-dimensional human body model. Results show that the path loss at a higher radio frequency is significantly smaller. Given that the transmitter and the receiver are located on the body trunk, the path loss relevant to the proposed minimum equivalent surface distance follows a log-fitting parametric model, and the path loss exponents are 4.7, 4.1 and 4.0 at frequencies of 2.4, 5.2, 5.7 GHz, respectively. On the other hand, the first-arrival delays are less than 2 ns at all receivers, and the maximum time delay spread is about 10 ns. As suggested by the maximum time delay spread, transmission rates of W-BSN must be less than 10^8 symbol/s to avoid inter-symbol interference from multiple-path delay.

Key words: channel model; path loss; time delay characteristics; wearable body sensor network

Next-generation mobile systems are evolving towards user-centric networks, where constant and reliable connectivity services are essential. With the development of various wearable wireless biosensors for mobile telemedicine applications, it is necessary to build up a wearable body sensor network (W-BSN) for interconnecting biosensors on an individual to improve system efficiency and reliability. For example, Knostantas et al. [1] in the MobiHealth project proposed an early prototype of body sensor networks, which was designed to monitor patients with different health care cases, including cardiac arrhythmia and respiratory insufficiency. In their prototype, wireless technologies like Bluetooth and Zigbee were used for inter-network communications. The Human ++ research project by IMEC aimed to provide an optimized sensor system for the personal body area network, where the ultra-wideband modulation was integrated into the sensor system[2].

For the low-power, reliable and robust on-body radio communication systems, a deterministic and generic channel model is required to provide a clear picture of the on-body radio propagation, including path loss and time delay characteristics. Though existing communication standards, such as IEEE 802.15.1/3/4 for wireless personal networks, have been adopted for some of these applications, there is in general a lack of research about on-body propagation, which is absolutely necessary for developing efficient W-BSN systems because the human body is a medium that poses numerous wireless transmission challenges.

Received 2006-11-30.

Foundation items: The High Technology Research and Development Program of Jiangsu Province (No. BG2005001), the Hong Kong Innovation and Technology Fund (No. ITS/99/02).

Biographies: Bao Shudi (1977—), female, graduate; Shen Lianfeng (corresponding author), male, professor, lfshen@seu.edu.cn.

1 Background

1.1 Previous studies

There are a number of studies characterizing and analyzing the on-body channels and also investigating the electromagnetic wave propagations around the body, among which, however, only a few concern the narrowband channel propagations at 2.4/5.2/5.7 GHz where most wireless standards operate.

Hall et al. [3] carried out measurements of the loss between two body-mounted antennas at 2.4 GHz, which showed significant variations that could be to some extent related to physiological changes in the body during the measurement period. Nechayev et al. [4] further carried out measurements on the propagation path gain for a number of antenna positions and at a number of static human body postures as well as during arbitrary movements. Their results suggested that the mean propagation gain for arbitrary antenna positions on a human body could be approximated by a power law with an exponent of −3.2. If both antennas were mounted on the trunk, on the other hand, an exponential law was followed closely. Roelens et al. [5] discussed the path loss between two half-wavelength dipoles near flat, biological tissue at 2.4 GHz. Both hom-

ogeneous and layered media were investigated. They found that the path loss near homogeneous tissue could differ significantly from the path loss near layered media.

Nevertheless, because of the very complex shape and internal structure of the human body, there have not been deterministic on-body channel models yet. Since the measurement results could be affected by many factors, such as body movements and physiological varieties, the simulation method is, therefore, indispensable as the way to reach an accurate model of such specific radio channels.

1.2 FDTD method

The finite-difference time-domain (FDTD) method, first proposed by Yee[6], is arguably the most popular numerical method for the solution of problems in electromagnetism, in that both space and time are divided into discrete segments and transient fields are computed as a function of time. Space is segmented into box-shaped cells known as Yee cells, each edge of which is small compared to the wavelength. The electric field intensity vectors, i. e. $\boldsymbol{E}_x$, $\boldsymbol{E}_y$ and $\boldsymbol{E}_z$, are located on the edges of the cell and the magnetic field intensity vectors, i. e. $\boldsymbol{H}_x$, $\boldsymbol{H}_y$, and $\boldsymbol{H}_z$, are positioned on the faces. Many Yee cells are combined together to form a three-dimensional volume, i. e. an FDTD mesh.

In this study, Remcom XFDTD is employed to model the properties of on-body radio propagation in three-dimensional space. In most cases, an XFDTD simulation will begin with the creation of the simulation space geometry. After all objects describing the geometry have been entered, the FDTD mesh can be created. With the geometry step finished, the desired inputs to the calculation may be defined. A wide range of output data may be saved, including both time-domain and frequency-domain values. Then, the calculation engine performs the actual FDTD calculations of the fields over the geometry mesh and saves the outputs specified.

In addition, a proper threshold of convergence in the time-domain must be ensured for accurate numerical results, which would enable the termination of calculation when converged. For example, for sinusoidally excited problems, typical values for this setting range from -55 to -25 dB depending on the level of accuracy versus runtime desired. As for the calculation stability, a free-space border of 10 to 20 cells is the best way to ensure the stability and accurate performance of the outer boundary for many problems.

2 Simulation Setup

2.1 Human body model

A human body model was set up with several different geometries: One sphere for the head ($r = 0.1$ m), one ellipse cylinder for the trunk ($a = 0.15$ m, $b = 0.12$ m, $h = 0.65$ m), two cylinders for arms ($r = 0.05$ m, $h = 0.70$ m), and two cylinders for legs ($r = 0.07$ m, $h = 0.85$ m), as shown in Fig. 1(a). It is well known that a real human body contains a variety of tissues with different values of relative permittivity and conductivity. For considerations of simplification, the trunk and limb parts of the body model are supposed with a shell of skin and a fill of muscle, while the head is considered with a shell of skin and a fill of brain. Tab. 1 gives the characteristics of these biological tissues at 2.4/5.2/5.7 GHz.

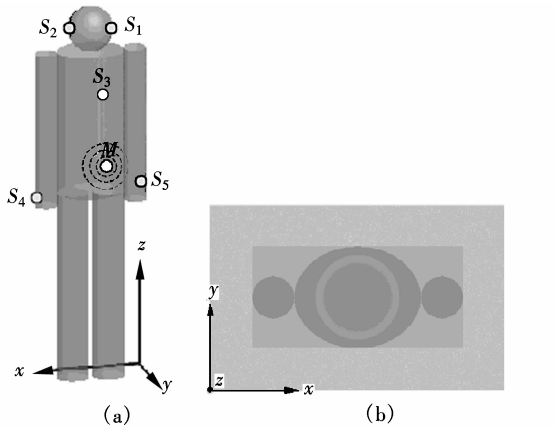

Fig. 1 Geometric human body model. (a) With locations of a transmitter and five receivers; (b) 2-D grid placement with geometry bounding box and mesh bounding box

Tab. 1 Dielectric properties of biological tissues[7]

Tissue	2.4 GHz		5.2 GHz		5.7 GHz	
	ε_r	σ	ε_r	σ	ε_r	σ
Skin (dry)	38.063	1.441	35.610	3.219	35.197	3.631
Average muscle	53.639	1.775	49.849	4.473	49.135	5.007
Average brain	42.610	1.481	39.049	3.664	38.435	4.142

2.2 Simulation environment

The simulation environment is free space with the three-dimensional human body, where the thickness of free space around the human body is 0.1 m on each side of the geometry, and the outer boundary is with artificial absorbing material. The entire simulation environment is meshed by $140 \times 88 \times 380$ cubic cells with each cell size being 5 mm. The two-dimensional grid placement with the geometry bounding box and the mesh bounding box is shown in Fig. 1(b).

2.3 Transceiver locations and feed specifications

The locations of transmitters and receivers are chosen based on commonly used on-body communication devices, such as headset and wristwatch, as shown in Fig. 1(a). Among the sensors, the one with less resource constraints acts as the master node of the W-BSN, denoted as M. Other sensors act as salve nodes, denoted as $S_i (1 \leqslant i \leqslant 5)$. In the simulation, the transmitting node M is located at the cell (94, 62, 230), and the

receiving nodes S_1 to S_5 are located at the cell (92, 48, 345), (49, 48, 345), (55, 68, 281), (19, 45, 200), and (123, 45, 200), respectively.

With regard to the feed specification at M, a discrete source with a single-frequency sinusoidal wave is deployed for steady-state results. The input source is series voltage with an amplitude of 1 V and a resistance of 50 Ω. Besides, discrete sources with a Gaussian pulse waveform are deployed for the simulation of time delay characteristics. The automatic convergence for all the calculations is set to a threshold of −30 dB. Finally, as the focus of this study is the signal attenuation through the medium from the transmitter to the receiver, the effects of antenna effects are not within the scope of this study.

3 Analysis of Simulation Data

3.1 Path loss

The received power P_{Rx} can be calculated from electric field intensity E(V/m) by

$$P_{Rx} = P_D \frac{\lambda^2 G}{4\pi} = \frac{E^2}{120\pi} \frac{\lambda^2 G}{4\pi} = \frac{E^2}{480\pi^2} \frac{c^2 G}{f^2} \quad (1)$$

where P_D is the power density in W/m^2, c is the speed of light through free space, and G is the antenna gain. Path loss in decibels is defined as $P_L(d) = -10\log_{10}(P_{Rx}/P_{Tx})$, where d is the distance in meters between the transmitter and the receiver, and P_{Tx} and P_{Rx} are the transmitted and received power, respectively[8]. Due to the important role of surface waves in such propagation environments, the relationship between the minimum surface distance d_s and the path loss will be studied.

Given that the antenna gain $G = 1$, the path loss at different frequencies is depicted in Fig. 2. It can be seen that the path loss at a higher radio frequency is significantly smaller. On the other hand, the minimum surface distances between M and S_1 to S_5 are about 0.77, 0.77, 0.32, 0.50 and 0.28 m, respectively. Obviously, there is no determinate relationship between the minimum surface distance and the corresponding path loss. The analysis will then be focused on the path loss in cases where the transmitter and the receiver are both on the trunk.

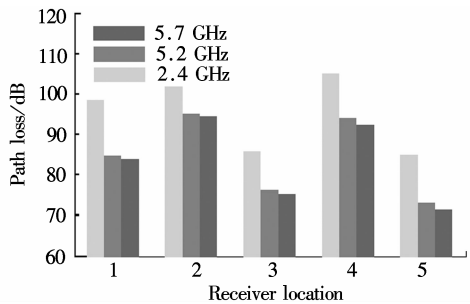

Fig. 2 Comparison of path loss at S_1 to S_5

First, let us look into the cases where the height of the locations of receivers is the same as that of the transmitter, i.e. $x_{Rx} \neq x_{Tx}$, $y_{Rx} \neq y_{Tx}$, $z_{Rx} = z_{Tx}$. Fig. 3 shows the relationship between the minimum surface distance and the corresponding path loss in such cases. A modified expression of the existing log-fitting parametric model[8], i.e.,

$$P_L(d_s) = P_L(d_{s0}) + 10\gamma_c \log\left(\frac{d_s}{d_{s0}}\right) + X_\sigma \quad (2)$$

can be adopted to characterize the path loss, where d_s is the minimum surface distance in millimeters between the transmitter and the receiver; d_{s0} is a close-in surface distance in millimeters for reference; γ_c is the path loss exponent; and X_σ denotes a zero-mean Gaussian random variable of standard deviation σ.

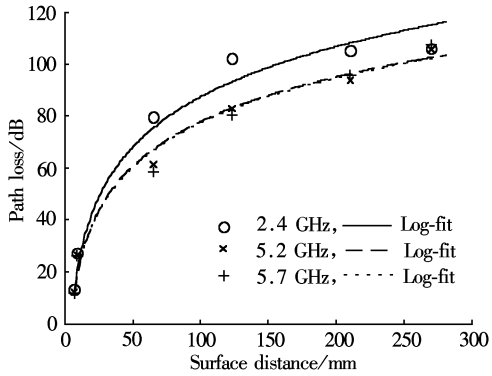

Fig. 3 Path loss in cases where Rx and Tx are on the trunk and $x_{Rx} \neq x_{Tx}$, $y_{Rx} \neq y_{Tx}$, $z_{Rx} = z_{Tx}$

Secondly, the path loss in cases where $x_{Rx} = x_{Tx}$, $y_{Rx} = y_{Tx}$, $z_{Rx} \neq z_{Tx}$ is depicted in Fig. 4. We fitted one log curve and one straight line minimizing the standard deviation to model the path loss. The linear-fitting model is expressed as

$$P_L(d_s) = P_L(d_{s0}) + \chi \frac{d_s - d_{s0}}{d_{s0}} + X_\sigma \quad (3)$$

where χ is the path loss slope. While only a log-fitting model is used to characterize the path loss in these cases, the deviations are larger but still acceptable.

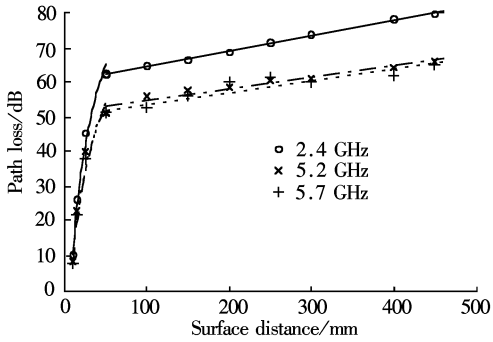

Fig. 4 Path loss in cases where Rx and Tx are on the trunk and $x_{Rx} = x_{Tx}$, $y_{Rx} = y_{Tx}$, $z_{Rx} \neq z_{Tx}$

Thirdly, the path loss in other cases, i. e. $x_{Rx} \neq x_{Tx}$, $y_{Rx} \neq y_{Tx}$, $z_{Rx} \neq z_{Tx}$, is depicted in Fig. 5. The log-fitting model is expressed as

$$P_L(d_{es}) = P_L(d_{es0}) + 10\gamma \log(d_{es}/d_{es0}) + X_\sigma \quad (4)$$

where

$$d_{es} = \sqrt{(d_l)^2 + (d_c)^{2\gamma_c/\gamma_l}} \quad (5)$$

is the equivalent minimum surface distance in millimeters between the transmitter and the receiver; d_{es0} is an equivalent close-in surface distance in millimeters for reference; d_l is the straight component of minimum surface distance; d_c is the curving component of minimum surface distance; and γ_c and γ_l are the path loss exponents in cases where ($x_{Rx} = x_{Tx}$, $y_{Rx} = y_{Tx}$, $z_{Rx} \neq z_{Tx}$) and ($x_{Rx} \neq x_{Tx}$, $y_{Rx} \neq y_{Tx}$, $z_{Rx} = z_{Tx}$), respectively. It should be noted that $d_s = \sqrt{(d_l)^2 + (d_c)^2}$. The parameter values of log-fitting curves of Fig. 5 are given in Tab. 2.

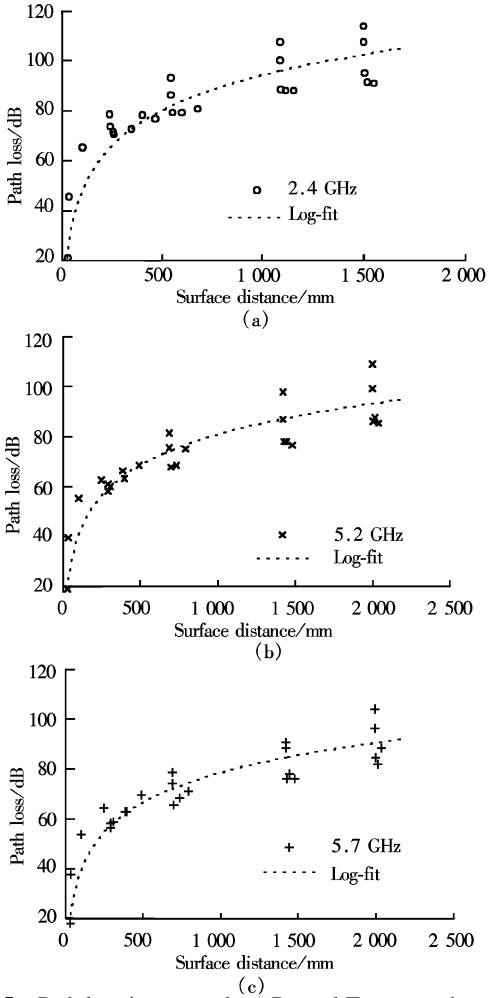

Fig. 5 Path loss in cases where Rx and Tx are on the trunk and $x_{Rx} \neq x_{Tx}$, $y_{Rx} \neq y_{Tx}$, $z_{Rx} \neq z_{Tx}$

Tab. 2 Parameters of log-fitting curves in Fig. 5

Parameter	2.4 GHz	5.2 GHz	5.7 GHz
γ	4.7	4.1	4.0
σ/dB	9.32	7.98	7.32

3.2 Time delay characteristic

Since impulse response can provide a wideband characterization of the propagation channel and contain all of the information necessary to analyze any type of radio transmission through that channel, in our simulation the transmitter was modeled as a discrete source of series voltage, which was a Gaussian waveform with a pulse width of 1 ns, and the simulating time step was set to $\Delta t = 9.6$ ps for stability. Fig. 6 shows the Gaussian waveform and its responses at the receiver locations S_1 to S_5, respectively. It can be seen that the response at S_2 has a larger value of time delay than those at the other receiver locations, while the amplitude at S_4 is smaller than the others. The first-arrival delay which is a time delay corresponding to the arrival of the first transmitted signal at the receiver is given in Tab. 3.

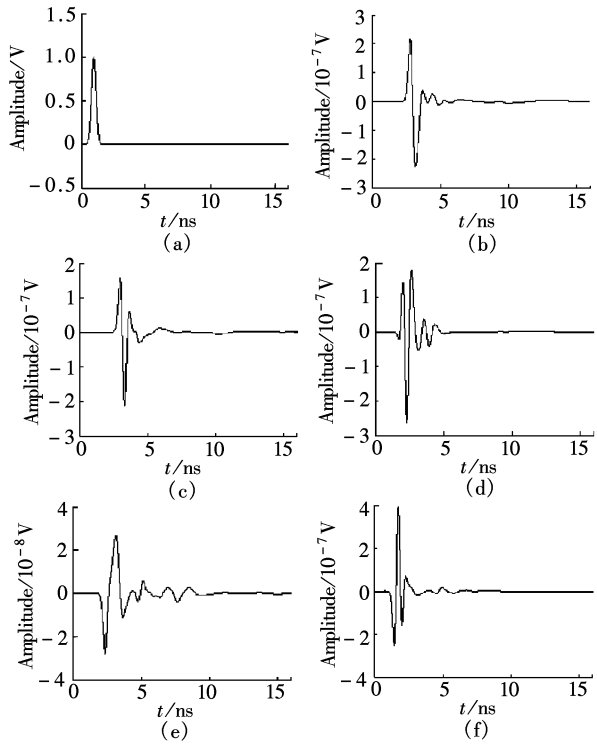

Fig. 6 Gaussian input and its responses. (a) Input at M; (b) Response at S_1; (c) Response at S_2; (d) Response at S_3; (e) Response at S_4; (f) Response at S_5

Tab. 3 First-arrival delay at receiver locations

Location	First-arrival delay/ns
S_1	1.78
S_2	2.01
S_3	0.99
S_4	1.37
S_5	0.47

Multiple-path delay is one of the main reasons for inter-symbol interference (ISI) in communication systems. If the difference in time delay between different paths is much smaller than the symbol period, such caused ISI would be negligible. As shown in Fig. 6, the maximum time delay spread is within 10 ns. Therefore,

in order to avoid ISI from multiple-path delay and reduce the receiver complexity, the transmission rate of W-BSN is suggested to be less than 10^8 symbol/s.

4 Conclusion

In this study, the on-body radio propagation of 2.4/5.2/5.7 GHz wearable body sensor networks has been characterized using Remcom XFDTD, including path loss and time delay characteristics. The results show that the path loss at a higher radio frequency is significantly smaller. As for the loss model, the numerical results indicate that the path loss relevant to the corresponding minimum surface distance of on-body channels between different transmitter and receiver locations differs a lot. In cases where the transmitter and the receiver are both located on the trunk, the path loss follows a log-fitting parametric model with the proposed equivalent minimum surface distance. And the path loss exponents are 4.7, 4.1, and 4.0 at frequencies of 2.4, 5.2, 5.7 GHz, respectively. As for the time delay characteristic, the first-arrival delay exhibits a positive relationship with the surface distance. To reduce the receiver complexity, transmission rates of narrowband W-BSNs are suggested to be less than 10^8 symbol/s to avoid ISI from multiple-path delay. Nonetheless, further studies need to be carried out to reach a comprehensive knowledge of complex on-body channels. The technology of ray tracing may be, for example, employed to fully evaluate the geometry effects.

References

[1] Konstantas D, van Halteren A, Bults R, et al. Mobile patient monitoring: the MobiHealth system [J]. *Journal on Information Technology in Healthcare*, 2004, **2**(5): 365 – 373.

[2] Gyselinckx B, van Hoof C, Ryckaert J, et al. Human + +: autonomous wireless sensors for body area networks [C]// *Proc of IEEE Custom Integrated Circuits Conf*. San Jose, CA, USA, 2005: 13 – 19.

[3] Hall P S, Ricci M, Hee T M. Measurements of on-body propagation characteristics [C]// *Proc of IEEE Antenna and Propagation Society Intl Symposium*. San Antonio, TX, USA, 2002: 310 – 313.

[4] Nechayev Y I, Hall P S, Constantinou C C, et al. On-body path loss variations with changing body posture and antenna position [C]// *Proc of IEEE Antenna and Propagation Society Intl Symposium*. Washington DC, USA, 2005: 731 – 734.

[5] Roelens L, Joseph W, Martens L. Characterization of the path loss near flat and layered biological tissue for narrowband wireless body area networks [C]// *Proc of IEEE Workshop on Wearable and Implantable Body Sensor Networks*. Boston, MA, USA, 2006: 50 – 56.

[6] Yee K S. Numerical solution of initial boundary value problems involving Maxwell's equations in isotropic media [J]. *IEEE Trans on Antennas and Propagation*, 1966, **14**(3): 302 – 307.

[7] Gabriel C. Compilation of the dielectric properties of body tissues at RF and microwave frequencies [EB/OL]. (1996-06-20) [2006-10-03]. http://www.fcc.gov/cgi-bin/dielec.sh.

[8] Sarkar T K, Zhong J, Kyungjung K, et al. A survey of various propagation models for mobile communication [J]. *IEEE Antenna and Propagation Magazine*, 2003, **45**(3): 51 – 82.

基于 FDTD 方法的 2.4/5.2/5.7 GHz 穿戴式躯域传感器网络体表信道特征分析

鲍淑娣[1,2]　沈连丰[1]　张元亭[2]

([1] 东南大学移动通信国家重点实验室,南京 210096)

([2] 香港中文大学生物医学工程联合研究中心,中国香港)

摘要:应用基于时域有限差分法(FDTD)的 XFDTD 仿真工具分析研究 2.4/5.2/5.7 GHz 穿戴式躯域传感器网络(W-BSN)的体表路径损耗和时延特性. 仿真环境为置于自由空间中的简化三维人体模型. 分析结果表明,当工作频率较高时,路径损耗相对较小;当发送点和接收点都置于主躯干时,路径损耗与最小等效体表距离遵循对数拟合模型,并且 2.4,5.2,5.7 GHz 下的衰减指数分别为 4.7,4.1 和 4.0. 另一方面,各接收点的首径延迟约小于 2 ns,而最大时延扩展为 10 ns. 为避免多径延迟引起的码间干扰,建议 W-BSN 的传输速率应小于 10^8 符号/s.

关键词:信道模型;路径损耗;时延特性;穿戴式躯域传感器网络

中图分类号:TN929.5